12 Simulations, Requirements, and Detector Performance

This chapter ties together the previous descriptive chapters and describes the performance we expect from the LZ apparatus. Our estimates of performance are based on detailed simulations, which have been substantially overhauled since completion of the LZ Conceptual Design Report [1]. The LUX collaboration has performed extensive high-statistics calibrations of ER background [2], NR signal [3], and implemented these calibrations in an improved analysis using the profile likelihood ratio technique [4] of the LUX WIMP search data [5].

We have incorporated the performance improvements made by LUX, which change the sensitivity in two principal manners:

1. The LZ sensitivity to low-mass WIMPs and to nuclear recoils from solar ^{8}B neutrinos is much improved.

2. The LZ sensitivity to sources of ER background, including, prominently, the "quiet" beta decay of daughters that trace their parentage to radon impurities, is much reduced.

12.1 Simulations

In this section we describe in detail the simulations used to develop the background and sensitivity studies presented in this report. The simulations were performed using LZSim, an offshoot of the LUXSim package originally developed for the LUX experiment and based on the GEANT4 particle physics simulation software [6, 7]. Designed specifically for low-background detector modeling, LZSim generates events and records particle interactions on a detector geometry component-by-component basis, but with an infrastructure independent of the detector geometry.

The LZSim infrastructure allows the user to define any detector component as a GEANT4 sensitive detector at run-time with a macro command. It incorporates internal bookkeeping to automate the generation of backgrounds arising from a variety of event generators, each with intensities set by the user at run time, and with a time-ordered stochastic primary event record. The geometry components are customized using coding techniques familiar to users of the base GEANT4 code. The event generators can be based either on the internal GEANT4 classes or created from scratch by the users. LZSim automatically records quality control information to a header in each output file to establish a record of how the data was generated.

We use GEANT4 version 4.9.5, the physics list `QGSP_BIC_HP`, and the libraries of CLHEP version 2.1.0.1. LZSim provides the option to incorporate the NEST model that describes ionization and scintillation formation for NRs and ERs [8, 9]. Currently we instead pass the output from LZSim to a standalone version of the NEST model that incorporates the latest results from the LUX experiment [2, 5].

12.1.1 Geometry construction

A detailed model of the LZ detector geometry was created within the LZSim framework according to CAD drawings of the detector. Components with significant mass or high amounts of radio-impurities as well as those located very close to the active xenon target are included. Elements that influence light collection and their respective optical properties are also described in the model.

Our model describes the detector from the outside in, with a few exceptions, nesting each successive volume or component within the one preceding it. The outermost volume is the steel water shielding tank. Placed within the water of the shielding tank are the major components of the outer detector of Chapter 4, including the segmented acrylic vessels, liquid scintillator, foam displacer, reflectors and R5912 PMTs. Services for the TPC such as the cryostat support stand, cathode high voltage conduit and thermosyphon and PMT cabling conduits require penetrations in the acrylic tanks that can impact veto performance and are therefore implemented in the detector model. Conduits that contain multiple or complex materials such as coaxial cable, gaseous or liquid xenon, and vacuum are modeled by a single material which represents the average density and composition of all materials in that conduit. Angled and horizontal neutron calibration tubes and a port for the YBe source are included for calibration source studies.

Located within the outer detector is the titanium cryostat, built according to the engineering models, as shown in Fig. 12.1.1. An inner cryostat vessel is contained within the outer cryostat vessel, also made of titanium and built to engineering specifications. The model includes multi-layer insulation between these two volumes, in addition to vacuum. No optical properties are defined between these regions as no photons are expected to be produced here.

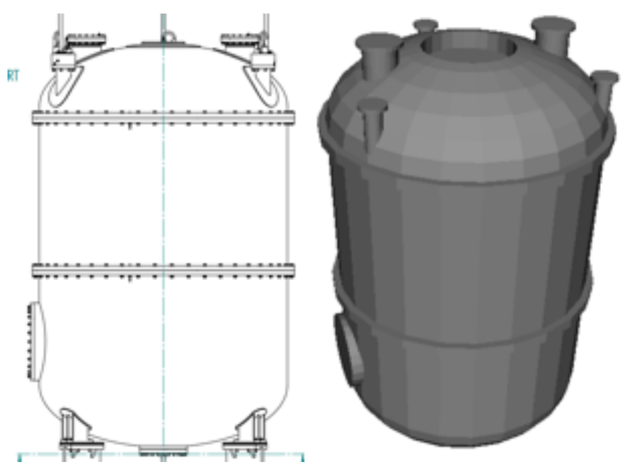

Figure 12.1.1: Engineering drawing and simulation geometry of the outer cryostat.

The first liquid xenon volume, known as the xenon skin, is just inside the inner cryostat vessel and continues inward to the outer surface of the TPC. The skin also extends below the bottom of the TPC through the bottom dome (see Chapter 3 for more details). The inner wall of the cryostat in the simulation is covered in a thin PTFE liner to aid light collection.

Optical boundaries, which can be defined at run time, are used between the liquid xenon skin and the components within to study the effects of changes in the assumed reflectivities.

The heart of the experiment, the liquid xenon TPC where the primary scintillation (S1) and secondary scintillation from ionization (S2) signals would be caused by a WIMP, is nested inside the skin volume. A rendering of the TPC is shown Fig. 12.1.2. The liquid xenon in the TPC is divided into two volumes. The active volume contains all the liquid xenon above the cathode, where well-reconstructed S1/S2 events occur. The second volume is the reverse field region (RFR), below the TPC cathode. Energy depositions in this volume cause an S1 signal, but no S2. Nevertheless, sometimes an RFR S1 signal becomes associated with an unrelated S2 signal, resulting in a class of events known as “gamma-X”. A third xenon volume, the gaseous xenon above the liquid where electroluminescence develops for the S2 signal, is also defined.

A cylinder of PTFE with extremely high diffuse reflectivity forms the TPC wall. Field shaping rings and grading resistors in the walls are represented. TPC components including the bottom shield grid, cathode grid, gate grid, and anode grid, according to the design described in Table 3.6.3, are represented. Optical boundaries between the liquid xenon and the PTFE walls as well as between the liquid xenon and the stainless steel of the grid wires are included to describe the light collection properties of the detector.

At the top and bottom end of the TPC cylinder are the PMT arrays, containing representations of each R11410 PMT that will be used in the LZ experiment. The PMTs are described as a stainless steel shell with vacuum inside. Materials representing the dynode chain are included to model the radioactivity of those components.

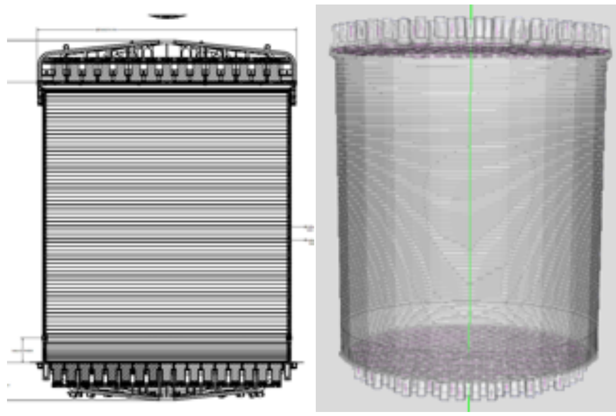

Figure 12.1.2: Engineering drawing and simulation geometry of the TPC

The face of the PMT is a quartz window with an additional thin layer of quartz buried within to represent the photocathode. The window and photocathode volumes are divided to model cases where a photon reflects off the front face of the PMT and fails to penetrate to the photocathode.

Optical interfaces at the top of the TPC between the PMT windows and gaseous xenon in the extraction region, and at the bottom array between the PMT windows in liquid xenon, are described so GEANT4 appropriately handles the reflection and transmission of photons. The PMT photocathode is defined as a GEANT4 sensitive detector to collect optical photons. The PMT array volumes also contain the support plates and support trusses that provide the mechanical support for the PMTs. Figure 12.1.3 shows a comparison between the current engineering design and the simulated geometry of the bottom PMT array.

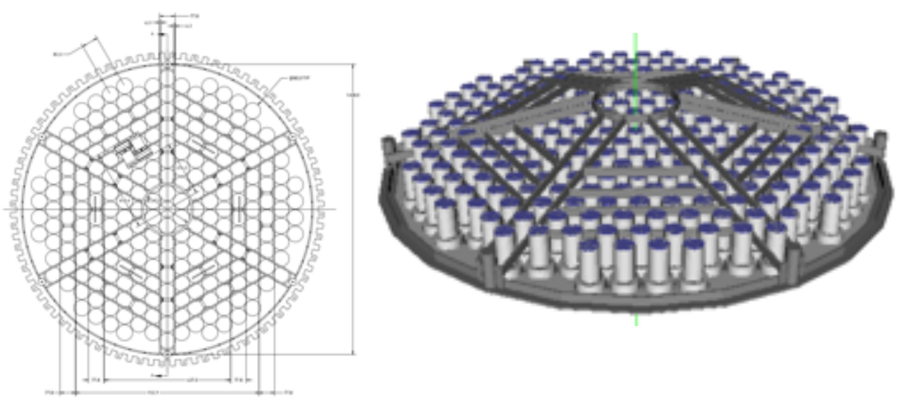

Figure 12.1.3: Engineering drawing and simulation geometry of the bottom PMT array and support truss. The skin PMTs that mount to this truss are not shown.

12.1.2 Event Generators

A variety of software packages are employed to simulate the physics of signals and backgrounds that induce responses in the LZ detector. The event generators which describe the WIMP signal and neutrino physics are derived from the references cited in Chapter 2. Here we discuss the event generators employed to describe various types of background phenomena in the LZ detectors.

12.1.2.1 Neutron production in detector materials

Neutrons emitted from radioactive processes in the material near to the LZ liquid xenon detector can create isolated nuclear recoils that might fake the recoils expected from WIMPs. To simulate neutron backgrounds from radioactivity (the ^{238}U, ^{235}U and ^{230}Th decay chains), LZSim uses input neutron spectra as calculated with the SOURCES-4A [10] package.

The SOURCES-4A code calculates neutron yields and spectra from spontaneous fission, (α,n) reactions and delayed neutron emission due to the decay of radionuclides. Its library contains all alpha emission lines from known radioactive isotopes. The code takes into account the energy losses of alphas, cross-sections of (α,n) reactions and the probabilities of nuclear transition to different excited states. We use an option for a thick target neutron yield allowing for calculation of neutron yields and spectra under the assumption that the size of a material sample exceeds significantly the range of alphas.

The original SOURCES-4A code has been modified [11–13] to extend the energy range of alpha particles to 10 MeV and to include (α,n) cross-sections and transition probabilities to excited states for most isotopes relevant to underground rare event experiments, based either on measurements or on EMPIRE1.19 [14].

The neutron spectra from SOURCES-4A are implemented as generators in LZSim, allowing any detector component to become a source of neutrons. For each component of interest, we simulate concentrations of 10 ppb of uranium or 10 ppb of thorium; these concentrations are then scaled to match the results of the materials screening. The uranium decay chains are split into early and late branches, and the ^{210}Pb sub-chain is calculated separately.

The spontaneous fission (s.f.) process is treated separately to exploit the ability of LZ to reject decays producing multiple neutrons and gammas, such as those produced in s.f. events. The SOURCES-4A package generates individual neutron spectra without accounting for simultaneous multiple neutrons and gamma rays. A special generator was developed to accurately simulate multiple neutrons (2.01 on average for ^{238}U) and gammas (6.44 on average for ^{238}U) in s.f. events. Accounting for multiple neutrons and gammas permits accurate description of multiple simultaneous signals in the LZ detector, and accurate accounting of the rejection of events with multiple signals. Most spontaneous fission events, particularly those in materials close to the LXe target, are rejected through their tendency to produce multiple hits.

12.1.2.2 Muon-induced neutrons

Energetic neutrons can be produced by atmospheric muons that penetrate to the rock around the Davis Cavern. Simulations of this process commence with the selection of muons with positions, directions, and energies sampled according to the MUSUN code [15] after transport using standalone MUSIC code [16]. MUSUN has been integrated into LZSim as a particle generator in such a way that events are generated from the surface of a cuboid surrounding the detector.

Muons sampled with the MUSUN code are then passed to GEANT4 which transports them and their secondaries including neutrons to the detector. All processes relevant to muon, photon, electron, and hadron interactions are included and the models are equivalent to those used in the GEANT4 physics list called Shielding, recommended by the GEANT4 developers for this application.

12.1.2.3 Gamma activity in large detector components

Background ER events from ^{40}K, ^{60}Co, and the ^{238}U and ^{232}Th decay chains are also modeled using a particle generator developed in LZSim. Ions of the parent isotopes are positioned in a component and the full decay chain is simulated according to the physics described by the GEANT4 radioactive decay data libraries. Crucially, the decay chain is produced in equilibrium, which allows splitting of the chain by individual isotopes during analysis. Thus, only one simulation is required, independent of the relative decay rates of individual radioactive isotopes within the chain. As for the neutron studies, fixed activities are simulated for each component, which are then renormalized based on materials screening results.

12.1.2.4 Gammas from the cavern rock

The external background from gammas in the rock walls of the cavern are also assessed using the radioactive decay chain generators described in the previous section. However, due to the large number of primary decays required to accumulate events in the active xenon, event biasing is used to boost statistics. This involves saving events at decreasing distances from the target and feeding them back into LZSim multiple times as primary particles. By default, LZSim records all hits within a detector component with a defined record level, but for these simulations the structure has been modified so that the output is recorded for tracks according to the distance from the center of the TPC. Additionally, modifications were made to allow the LZSim binary output files to be input as primary particles.

12.1.2.5 Benchmark points

A new generator has been developed to allow the assessment of the impact of the radioactivity of small size components (e.g. sensors) quickly. LZSim was designed to primarily distribute primary events throughout a given volume. Our new generator can associate radioactive events with a specific geometric location (the 'Benchmark Point') within the LZSim geometry.

12.1.3 From energy deposition to signals

The event generators described in the previous section are used to generate different radioactive decay products. These particles are tracked by GEANT4 as they deposit their energy in different volumes of the geometry. LZSim allows any part of the volume to be a sensitive detector, and for these simulations, we record all depositions in the TPC, as well as associated energy depositions in the skin region and the outer detector. Among the data saved in each volume for each event are the locations, times, and magnitudes of energy deposits made by various particle types.

In the skin and TPC liquid xenon volumes, energy depositions within 400 μm are clustered (to encompass the largest possible ER and NR track sizes) and categorized as either ER or NR depending on the interaction. The result is a list of energy-deposition clusters from a given particle type (ER or NR). The energy and associated particle type of each cluster as well as the local electric field are then fed into the NEST (Noble Element Simulation Technique) [8, 9, 17] package which stochastically computes the number of expected photons and electrons produced at each cluster.

NEST models the scintillation light and ionization charge yields of nuclear and electron recoils as a function of electric field and energy or $\mathrm{d}E/\mathrm{d}x$. NEST also models the drift, diffusion, absorption, extraction, and electroluminescence of the electrons as they move through the liquid and gas. "NEST" refers both to a collection of microscopic models for energy deposition in noble elements and to the Monte Carlo simulation code that implements these models. NEST provides mean yields and intrinsic fluctuations due to the physics of excitation, ionization, and recombination, including both Gaussian and non-Gaussian components of the energy resolution.

The NEST methodology was initially trained on data from a small dual-phase detector from Case Western Reserve University (Xed), which yielded comprehensive data sets in terms of energy range and field sweep [18]. The NEST model used in this simulation has been updated to incorporate the latest calibration results from the LUX experiment [2, 3, 5].

After the clustered energy depositions have been converted from energy to quanta (scintillation photons and ionization electrons) via the NEST models, a detector model is applied to convert these raw quanta into the detector observables, that is, into S1 and S2.

The primary scintillation light from the NEST models is propagated to the faces of the PMTs, accounting for binomial fluctuations, using the light collection model, including Fresnel transmission and reflection, described in Section 3.5. We refer to the average light collection efficiency as α_1, which the optical model currently predicts to be 8.5 % (better than our baseline value and requirement of 7.5 %), and we correct the raw signal (denoted S1) for the variation of light collection with position in the detector (denoted S2). Photoelectron production at the photocathode accounts for the double-photoelectron phenomenon described in [19]. A trigger requirement of three-fold coincidence of PMT hits is applied prior to subsequent analysis. Both S1 and S1c are reported to the user.

The S2 signal is produced from the number of ionization electrons that drift away from the interaction site. The LZ extraction efficiency (see Table 3.6.1) is applied to determine how many electrons are extracted to the gas phase. The extracted electrons are converted to a number of luminescent photons with NEST, accounting for LZ parameters, and these photons are then converted into photoelectrons at the PMTs. The S2 signal is also corrected for the position of the event in the detector, including the effect of non-infinite electron lifetime presumed in LZ to be 850 µs (corresponding to an absorption length of greater than 1.5 m). The raw and corrected signals, denoted S2 and S2c, are reported to the user.

In the central TPC the energy-weighted position and variance of all energy clusters is computed. The total S1 signal in the central xenon volume includes the S1 signal created by energy deposits in the reverse field region (RFR) below the cathode. Here, the electric field drifts electrons downward, making no contribution to the S2 signal.

A similar procedure is followed to model the S1 signal observed in the skin region (excluding S2 as no charge is collected in the skin). A light collection model is determined by simulating photons throughout the skin. Each energy deposit in the skin is converted into photon quanta using an electric field model of the skin and the NEST package. These photons are then converted to detected photoelectrons, and the final skin S1 is reported to the user.

The process that translates energy depositions into observed S1c and S2c signals does not currently account for PMT or DAQ electronics noise. A more complete model incorporating all known sources of noise leading to the generation of simulated waveforms is under development.

A substantial effort has gone into simulating the light collection for the outer detector liquid scintillator system. Currently, however, for the primary TDR physics simulations, only energy depositions from GEANT4 in the outer detector are used. The transport, capture, and conversion to gamma rays and nuclear recoils of neutrons are simulated in GEANT4.

12.1.4 Analysis cuts

For each event, we have a tree containing the energy and location of interactions in the TPC, the skin region, and the outer detector, and energy depositions in liquid xenon have been translated into raw and corrected S1 and S2 as described in the previous section. We apply a set of cuts to the simulation data to determine the backgrounds produced by a given radioactive decay chain in a given detector component. The baseline cuts that are used to produce the numbers in Table 9.2.7 are as follows:

- Region of Interest: $0 < \mathrm{S1c} < 20$ detected photoelectrons, but assuming 3-fold coincidence in the TPC PMTs. In other words, three PMTs have to have observed light, but the total sum of the signal can be arbitrarily small. For ER, this range is approximately 1.5 to 6.5 $\mathrm{keV_{ee}}$, and for NR, this range is approximately 6 to 30 $\mathrm{keV_{nr}}$. In addition, the uncorrected S2 signal is required to be >350 detected photoelectrons (5 emitted electrons) ensuring adequate signal size for position reconstruction.

- Single scatter event: $\sigma_Z < 0.2$ cm and $\sigma_r < 3.0$ cm. The energy-weighted variance in position must be less than the expected spatial resolution of the detector for an event to be classified as a single scattering event. The given values are based on the LUX performance with an estimated scaling to LZ. Gamma-X events are treated as single scatters, as no S2 can be observed from the second interaction vertex.

- Skin cut: <3 detected photoelectrons in the skin veto region, to ensure that no visible energy is deposited in the skin within the 800 µs coincidence window.

- Outer detector cut: <200 $\mathrm{keV_{ee}}$ deposited in the outer detector, to ensure that no visible energy is observed in the outer detector within the 500 µs coincidence window.

- Fiducial volume cut: the fiducial volume is defined as 4 cm from the TPC walls, 1.5 cm from the cathode grid and 13.5 cm from the gate grid, corresponding to 5.6 tonnes of LXe.

In some cases, particularly for the simulation of gamma backgrounds, adequate statistics could not be generated due to limitations in time and available disk space. In these cases, the upper bound of the region of interest was increased to 100 $\mathrm{keV_{ee}}$ to increase the statistics in the analysis. This scaling is only valid if the spectrum of background events is roughly flat below 100 $\mathrm{keV_{ee}}$; in the fiducial volume used here, this condition was met.

12.1.5 Validation

To ensure that the simulations are an accurate reflection of the detector design, the simulation code and outputs are validated in several ways. First, because the LZSim simulation package shares a code base with LUXSim, the extensive validations of LUXSim that have been performed using LUX data can be incorporated directly into LZSim. Therefore, the GEANT4 physics list, event generators, and the NEST models are vetted against LUX data before being applied to the LZ detector model.

Where possible, specific predictions of LZSim are validated against external, independent models. For example, the light collection studies described in Sec. 3.5.1 are produced using the full LZSim model, but are checked against an independent, MATLAB-based ray tracing code package developed by collaborators within LZ. Similarly, the parameters that drive the S2 photon detection described in Sec 3.6 are compared with results from independent electron transport models that are validated against LUX S2 pulses.

To validate the detector geometry, all components are checked against engineering drawings by at least two people. Given the high level of confidence in the optical model, based on the agreement with LUX data and the independent checks, the light collection models are used as a second validation step. The majority of mistakes in implementing the geometry become immediately apparent when looking at the predicted light collection. Before a modification to the geometry can be accepted into the repository, any changes to the light collection output that result from that modification are studied and understood.

Finally, a set of high-level cross-checks provides additional quality assurance for the key simulation results used for background rate estimates. These include comparisons to back-of-the-envelope calculations for the dominant sources of background, comparison of the SOURCES-4A neutron yields to those from an alternative simulation package, and sanity checks of neutron and gamma attenuation lengths along critical paths throughout the LZ geometry. All cross-checks are consistent with the full simulations output at a level that does not impact the LZ sensitivity requirement.

12.2 Requirements

In this section, we summarize the key requirements for the LZ experiment. The LZ collaboration has established a small number of requirements to guide and evaluate the design and fabrication of the detector systems.

The top-level scientific requirement is the sensitivity to WIMP dark matter, via the spin-independent scattering process. Subsidiary high-level science requirements and the flow-down from the overall sensitivity are shown in Fig. 12.2.1. The high-level requirements, including the key infrastructure requirements, are summarized in Table 12.2.1. These requirements flow down to the detector subsystems and are captured in a concise form available to the collaboration. There are two practical high-level requirements. First, all equipment and subassemblies must be transported via the Yates shaft (see Chapter 10), which imposes dimensional and weight limits. Second, the existing water tank now housing the LUX detector will be reused. The collaboration has also captured the requirements for detector subsystems at WBS Level 2.

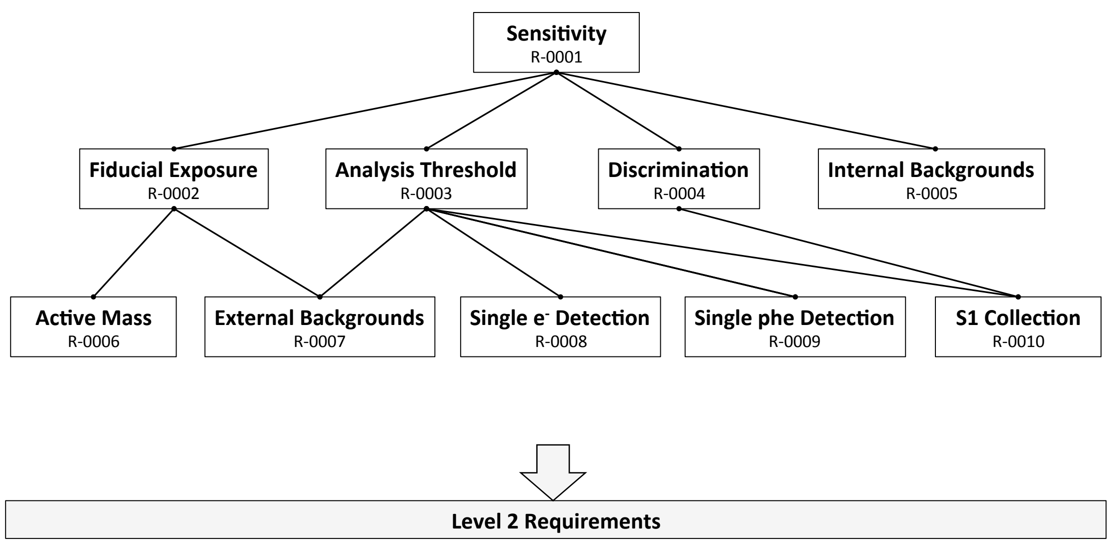

Figure 12.2.1: Flow down of the top level scientific requirements.

Requirements development and explication have been key elements of internal reviews of LZ detector systems and will be an important aspect of configuration control. All top-level and Level-2 requirements have been developed and reviewed in dedicated meetings. The requirements are captured in a Google document, along with additional material and documentation for each relevant WBS Level-2 element. The LZ instrument scientist and chief and deputy chief engineers (see Chapter 13) are primarily responsible for the maintenance of the requirements and their further development, if required, in close collaboration with the Level 2 managers.

Table 12.2.1: LZ Top Level Science Requirements

Number	WBS	Requirement Name	Requirement Description	Rationale
Primary				
R-0001	Science	WIMP Sensitivity	Sensitivity to 40 GeV/c^2 WIMPs is 3×10^{-48} cm^2 or better	Probe limit of liquid xenon technology set by solar neutrino background. Approach sensitivity to atmospheric neutrinos. Test supersymmetric and extra-dimension models of dark matter
Secondary				
R-0002	Science	Fiducial Exposure	Minimum of 5,600 tonne-days	Needed to achieve sensitivity requirement. Achievable with fiducial mass of 5.6 tonnes and assumed running period of 1,000 live days or less fiducial mass and longer running time
R-0003	Science	Analysis threshold	50 % efficiency at 6 keV$_{nr}$	Probe WIMP mass range down to 5 GeV/c^2 with non-negligible sensitivity
R-0004	Science	ER Discrimination	99.5 % ER discrimination for 50 % NR acceptance	Limit background from ERs so as to reach WIMP sensitivity requirement
R-0005	Science	Internal backgrounds	Internal backgrounds from radioactive noble gases (Rn, Kr, Ar) not to exceed four times the solar neutrino ER background	Limit ERs from internal backgrounds to an acceptable level. Solar neutrino rate does not include ^{8}B
Tertiary				
R-0006	Science	Active mass	7.0 tonnes	Required to reach fiducial exposure
R-0007	Science	External backgrounds	Backgrounds from radioactivity of the detector components (not including internal backgrounds, R-0005). ER counts before discrimination <25 and NR counts before discrimination <0.7	ER counts constrained to be <10 % of ERs from solar neutrinos (not including ^{8}B), including uncertainty in this rate. NR events to be constrained to be comparable to neutrino rate. We rely on veto efficiency to reduce the NR rate contribution. This rate, and to a lesser extent external ER contributions, define the fiducial mass. Analysis threshold also depends on size of these backgrounds.
(continued on next page)				

Table 12.2.1: (continued)

Number	WBS	Requirement Name	Requirement Description	Rationale
R-0008	Science	Single electron detection	50 S2 photoelectrons detected per emitted electron	Sufficiently large S2 signal for accurate reconstruction of peripheral interactions, such as those arising from contamination on the TPC walls.
R-0009	Science	Single photoelectron detection	Single S1 photoelectron detection with >90 % efficiency, so as to reach >70 % efficiency for 3 phe	Main determinant of analysis threshold.
R-0010	Science	S1 light collection	Volume-averaged S1 photon detection efficiency (geometric light collection times effective PMT quantum efficiency) of >7.5 %	Good discrimination and low energy threshold, equal or better than past Xe experiments. Exponentially falling (in recoil energy) WIMP spectrum means more recoils at lower energies, and low-energy recoils produce less S1 (both total and per-unit-energy) driving the S1 light collection efficiency requirement.
Infrastructure				
R-0100	General	All parts fit down Yates shaft	All detector elements must be sized so that they can be lowered via the Yates shaft	Yates shaft is primary access to the Davis campus
R-0110	General	Reuse Davis water tank	Existing Davis water tank is reused. Include minor modifications and refurbishment.	Not practical or cost effective to replace water tank. Insufficient underground space to make larger tank.

The baseline design described in this Technical Design Report meets or exceeds all requirements. We briefly summarize the key requirements by WBS element in the subsections below. Linkage among the various requirements has been part of the requirements review process.

12.2.1 WBS 1.1 Xenon Procurement

There is a single requirement for WBS 1.1 Xenon Procurement, that being to procure 10 total tonnes of xenon. This requirement flows down from R-0006, as 10 total tonnes are adequate to result in 7 active tonnes in the detector.

12.2.2 WBS 1.2 Xenon Vessel

The primary requirements for the cryostat vessels are shown in Table 12.2.2. The size of the cryostat determines the amount of target that can be deployed and flows down from the top level science requirement but also the infrastructure requirement that all parts must fit in the Yates shaft. The cryostat vessels must also be low radioactivity. Safety considerations dictate that the vessels are compliant with standard engineering codes.

Table 12.2.2: Level 2 Requirements for WBS 1.2 Xenon Vessel

Number	WBS	Requirement Name	Requirement Description	Rationale
R-120001	1.2	Inner Cryostat Vessel (ICV) Maximum Outer Diameter	Inner cryostat outside diameter less than 1.702 m (67.0 inch). Ports must be at angles where there is sufficient clearance.	Must fit within Yates shaft.
R-120002	1.2	Inner cryostat vessel (ICV) compact geometry	Design compact ICV to minimize use of passive xenon: ICV conical section and ellipsoidal 3:1 dished end	Saving xenon
R-120003	1.2	Outer Cryostat Vessel segmented	No fabrication underground	Segmented OCV fits into Yates shaft
R-120004	1.2	Low radioactivity of the cryostat material	Radioactivity budget from background simulations. Maximum contribution to the overall background: 3.3 % of pp solar neutrinos and 0.03 NR event	Low radioactivity, low density minimizing, efficiency of Outer Detector
R-120005	1.2	Outer Cryostat Vessel (OCV) and Inner Cryostat Vessel (ICV) designed for 1.48 bar external pressure and vacuum internal	Working conditions for OCV and most severe failure mode for ICV	Vacuum inside and water outside
R-120006	1.2	Inner Cryostat Vessel (ICV) designed for 4 bar inner pressure and vacuum external	ICV working conditions	Xe gas inside with maximum pressure - including hydrostatic pressure at the bottom dished end; 3.4 bar top head
R-120007	1.2	Design compliance to codes	Compliance to ASME BPVC code VIII, 2012 Int. Building Code, ASCE 7 with soil classification Cals B for seismic conditions, Fabricator holds U-stamp certificate	Required by SURF SD regulations

12.2.3 WBS 1.3 Cryogenic System

The primary requirements for the Cryogenic System are shown in Table 12.2.3. The main objective of this system is to enable safe and efficient cooling of the LXe target volume. In particular, the cooling power must be adequate to enable rapid circulation of the Xe volume for purification to satisfy the Level-2 requirements in WBS 1.4, which is an example of linkage between WBS requirements.

Table 12.2.3: Level 2 Requirements for WBS 1.3 Cryogenic System

Number	WBS	Requirement Name	Requirement Description	Rationale
R-130001	1.3	Sufficient cooling power	Cryogen cooling systems shall be sufficient to remove heat for 500 slpm of Xenon circulation; purge of the detector Xenon gas space; and thermal losses of all the system components.	There must be adequate cooling to liquefy Xenon within the parameters of flow required to attain purity.
R-130002	1.3	Oxygen deficiency hazard safety	Engineered controls shall be implemented to achieve ODH Class 2 or better.	SURF requires ODH Class 2 or better for all experimental implementations
R-130003	1.3	Pressure safety - valves	Redundant relief devices shall be employed for pressure safety. Relief devices shall be sized per CGA S-1.3.	Properly sized redundant relief devices are a primary engineered control for pressure systems.
R-130004	1.3	Pressure safety - monitoring	Active pressure monitoring shall be utilized such that alarms provide warning of pressure going higher than the planned operating pressure range.	Monitoring of pressure may provide an opportunity to act on elevated pressure before one of the primary safety devices is activated.
R-130005	1.3	Materials	Materials exposed to LN temperatures shall be: a) low carbon stainless steel; b) aluminum based alloys; c) nickel based alloys; d) copper / copper based alloys; or e) pure titanium.	These materials will remain ductile at 77 K.
R-130006	1.3	Thermal insulation	Equipment at 175 K shall have a minimum of 10 layers and equipment at 77 K shall have a minimum of 25 layers of multi-layer insulation (MLI).	MLI is the most effective method of minimizing radiative heat load. Lower operating temperatures require additional layers of MLI.

12.2.4 WBS 1.4 Xenon Purification

The primary requirements for WBS 1.4 Xenon Purification are shown in Table 12.2.4. These requirements primarily flow down from R-0003 and R-0005, as the Xe must be pure enough to enable efficient extraction of signals to satisfy the analysis threshold requirement but also low enough in internal radioactive sources like Kr and Rn to satisfy the internal backgrounds requirement.

Table 12.2.4: Level 2 requirements for WBS 1.4 Xenon Purification

Number	WBS	Requirement Name	Requirement Description	Rationale
R-140001	1.4	Xe electronegative purity	Charge absorption length >1.5 m, O_2 equivalent =0.4 ppb.	Collect charge and scintillation throughout the entire volume of the TPC.
R-140002	1.4	Removal of Kr and Ar from Xe.	Ability to remove natural Kr from the Xe to a concentration of <0.015 ppt g/g. Ability to remove natural Ar from the Xe to a concentration of <0.45 ppb g/g.	Limit ER Background from ^{85}Kr and ^{39}Ar.
R-140003	1.4	Control the ingress of ^{222}Rn into the Xe	Control the decay rate of ^{222}Rn in the Xe.	ER background from ^{214}Pb. Limit the ^{222}Rn decay rate in the active Xe to 13.4 mBq.
R-140004	1.4	^{127}Xe activity	88 µBq/kg activity in the 5.6 tonnes fiducial volume at the start of physics data taking.	No more than 23 single-scatter events below 6 keV_{ee} from ^{127}Xe in the lifespan of the experiment.
R-140005	1.4	Safe Xe recovery	Safe recovery of the Xe during normal operations and during an emergency	Protection of the Xe investment.

12.2.5 WBS 1.5 Xenon Detector System

There are several requirements in WBS 1.5 Xenon Detector System. For example, the TPC must be large enough to accommodate the required target mass, the electric fields need to be adequate to achieve efficient single electron detection and to achieve the required 99.5 % ER/NR discrimination, the TPC must have adequate light collection, and the detector components must be made from clean materials to limit the external backgrounds seen by the LXe. R-150009 is another good example of the linkages between different WBS systems, as the power dissipated in the detector must be low enough that the cooling power specified in R-130001 is adequate. The primary requirements for WBS 1.5 Xenon Detector System are listed in Table 12.2.5.

Table 12.2.5: Level 2 Requirements for WBS 1.5 Xenon Detector System

Number	WBS	Requirement Name	Requirement Description	Rationale
R-150001	1.5	TPC inner dimensions	Dia. =1,456 mm / length =1,456 mm	7 tonne active mass, optimal self-shielding
R-150002	1.5	TPC drift field	300 V/cm	99.5 % discrimination; drift time <1 ms
R-150003	1.5	Electroluminescence field (GXe)	10 kV/cm	95 % emission; 50 phe/e^-; e-trains; wall events
R-150004	1.5	Energy resolution	2.0 % at 2.5 MeV (S1+S2)	Gamma spectroscopy for background model
R-150005	1.5	LXe Skin threshold	100 keV$_{ee}$ with 3 phe in >95 % of skin volume	Veto efficiency required for fiducial mass
R-150006	1.5	Component radioactivities	< 250/240/240/540 mBq U/Th/Co/K	<0.4 NR cts, <10 % pp neutrino ER cts (matches R-200114 to R-200117)
R-150007	1.5	Photocathode coverage	38 % top and bottom arrays	S1 Photon detection efficiency, vertex resolution, discrimination
R-150008	1.5	PTFE reflectivity	>95 % in LXe	Light collection efficiency in TPC and Skin
R-150009	1.5	Total heat in or on cryostat	140 W	Cooling power requirement, fluid model
R-150010	1.5	Max field for cathodic surfaces	50 kV/cm	Limit spurious photon/electron emission

12.2.6 WBS 1.6 Outer Detector

WBS 1.6, the Outer Detector, acts as the main neutron veto, and therefore most requirements in this WBS flow down from R-0007. The Level 2 Requirements for WBS 1.6 Outer Detector are shown in Table 12.2.6.

Table 12.2.6: Level 2 Requirements for WBS 1.6 Outer Detector

Number	WBS	Requirement Name	Requirement Description	Rationale
R-160001	1.6	Neutron veto efficiency	Detection efficiency of 95 % for a 1 MeV neutron that scatters once in the xenon	Needed to meet the neutron part of requirement on external backgrounds
R-160002	1.6	Outer Detector threshold	Threshold of 200 keV (50 % efficiency) on energy deposit in liquid scintillator	Highest achievable veto efficiency with acceptable deadtime
R-160003	1.6	Number of photoelectrons detected per energy deposit	>80 phe/MeV	Corresponds to about 15 phe at threshold of 200 keV
R-160004	1.6	Light collection efficiency	Efficiency of >5 % for having VUV photons strike a PMT	Light detection is proportional to light collection efficiency.
R-160005	1.6	Deadtime	OD must not veto more than 5 % of the WIMP search livetime	Keep overall activity low to limit deadtime imposed by OD veto triggers

12.2.7 WBS 1.7 Calibration System

The Calibration System must provide accurate calibrations of the light and charge yields, position dependencies, time variations, energy threshold, resolution, and discrimination parameters of the central TPC without taking an undue amount of running time away from the primary dark matter search. The Calibration System must also provide an accurate picture of the performance of the veto systems: the Xe skin and Outer Detector. The L2 requirements for WBS 1.7 Calibration System are listed in Table 12.2.7.

Table 12.2.7: Level 2 Requirements for WBS 1.7 Calibration System

Number	WBS	Requirement Name	Requirement Description	Rationale
R-170001	1.7	Calibration Times	<12 hrs/week for periodic calibrations and <100 d total for infrequent calibrations	12 hrs can fit in a single day of SURF operations (2 shifts). 100 days is 10 % of total exposure target.

(continued on next page)

Table 12.2.7: (continued)

Number	WBS	Requirement Name	Requirement Description	Rationale
R-170002	1.7	Calibrate TPC (x,y,z) variation	<2 % uncertainty on S1 and S2 mean area (of a monoenergetic peak) in bins of 5x5x5 cm	Understand detection efficiencies and gains at scales relevant to variation
R-170003	1.7	Calibrate ER band	<2 % uncertainty on the measured ER band mean and $\pm 1\sigma$ contours (in 1 phd bins of S1)	Clearly define ER background region
R-170004	1.7	Calibrate NR band	<2 % uncertainty on the measured NR band mean and $\pm 1\sigma$ contours (in 1 phd bins of S1)	Clearly define signal region
R-170005	1.7	Calibrate NR response at threshold	<5 % uncertainty on energy at 50 % acceptance	Clearly define threshold and map out ^{8}B neutrino response
R-170006	1.7	Calibrate TPC, skin and LS signal time offsets	$< \pm 1$ sample uncertainty in primary scintillation rise time jitter across the three analog electronics chains	Necessary for optimal veto efficiency
R-170007	1.7	Calibrate temporal response	<2 % uncertainty in S2 mean area (of a monoenergetic peak) in z-direction bins of 5 cm	To ensure stable energy reconstruction
R-170008	1.7	Calibrate Xe skin energy response	<2 % uncertainty on ER phd/keV (1 cm z bins) in Xe side skin	Understand skin threshold
R-170009	1.7	Calibrate energy scale of LS	<2 % uncertainty on ER phd/keV (volume-averaged) at 2.2 MeV	Verify outer detector performance
R-170010	1.7	Calibrate NR response	<5 % uncertainty on energy at about 30 keV	Bound the upper end of the WIMP-search range
R-170011	1.7	Calibrate fiducial volume fraction	<5 % uncertainty on fraction of TPC LXe mass satisfying fiducial selection criteria	Directly scales exposure and sensitivity

12.2.8 WBS 1.8 Electronics, DAQ, Controls, and Computing

The primary requirements for WBS 1.8 Electronics, DAQ, Controls, and Computing are shown in Table 12.2.8. The main requirement here is to enable a low energy threshold in the detector. However, there are two requirements that flow across from WBS 1.7, as the data acquisition must be robust enough to handle the event rates listed in Table 12.2.7 needed to effectively calibrate the detector. On the controls side, this subsystem is responsible for providing monitoring and control during emergencies, and in particular the control of the xenon recovery system of WBS 1.4.

Table 12.2.8: Level 2 Requirements for WBS 1.8 Electronics, DAQ, Controls, and Computing

Number	WBS	Requirement Name	Requirement Description	Rationale
R-180001	1.8	Energy threshold	90 % efficiency for a single phe	The S1 analysis threshold is defined by our efficiency to capture single-photoelectron signals. For a specific gain, this requirement fixes the noise requirements of the electronic chain. This calculation depends sensitively on the assumed 35 % variations in the PMT response.
R-180002	1.8	Source count rate	150 Hz	Able to handle source calibrations. Rates are limited by the drift time.
R-180003	1.8	LED count rate	4 kHz	Able to handle LED calibration rates.
R-180004	1.8	Guarantee the safety of xenon supply and the xenon circulation system	Use Programmable Logic Controllers (PLCs) to control and monitor the xenon purification, circulation, and storage systems	PLCs are used to ensure that the detector and xenon system are maintained in a safe state during emergencies that result in a shutdown of the slow-control infrastructure. The PLC system provides continuous real-time monitoring and control of the critical subsystems and will initiate automatic recovery of the xenon to the storage facility during an emergency.

12.2.9 WBS 1.9 Integration and Installation

The primary requirements for WBS 1.9 Integration and Installation are shown in Table 12.2.9. There are two main requirements in this WBS. The first is that all parts must be installed correctly, and the second is that the detector must be installed with clean parts in such a way to minimize exposure to radon and dust. These requirements flow down from the top level science requirements, particularly R-0005 and R-0007.

Table 12.2.9: Level 2 Requirements for WBS 1.9 Integration and Installation

Number	WBS	Requirement Name	Requirement Description	Rationale
R-190001	1.9	Parts used have acceptable radioactivity	All parts have a traceable history that shows they have low enough radioactivity to be used. This will be documented in a database and there will be an acceptance sheet with sign off that the part is usable.	Control background level in the experiment
R-190002	1.9	Parts used are clean	All parts have a cleaning procedure to ensure surface contamination is at an acceptable level. This will be documented in a database and there will be an acceptance sheet with sign off that the part is usable.	Control background in the experiment. Control contamination of Xenon that would reduce electron drift length and/or increase light absorption
R-190003	1.9	Parts are moved and lifted without damage	Moving and lifting will be done to procedures written and approved by subsystem experts. This will include analysis of rigging attachment and support loads where applicable. Workers will review the procedures and have rigging experience	Detector is assembled without damaging parts
R-190004	1.9	Parts are correctly assembled	Assembly work will be done to procedure written and approved by subsystem experts. Workers will review the procedure and have training where necessary.	Detector is assembled correctly
R-190005	1.9	Control Part exposure to Radon	Parts have an allowable total exposure to Radon, based on material and location. Monitored time of exposure and Radon level of air are recorded in a database. For critical parts, may use samples.	Control background level in the experiment

12.2.10 WBS 1.10 Cleanliness and Screening

The primary requirements for WBS 1.10 Cleanliness and Screening are shown in Table 12.2.10. At Level 2, the WBS 1.10 requirements dictate that the project has the sensitivity and capacity to screen all detector components at the level needed to ensure that the radioactivity requirements are satisfied. WBS 1.10 also keeps track of allowed radioactivity levels for individual components, and more details can be found in Chapter 9.

Table 12.2.10: Level 2 Requirements for WBS 1.10 Cleanliness and Screening

Number	WBS	Requirement Name	Requirement Description	Rationale
R-200001	1.10	Assay Sensitivity for U and Th by Direct Counting	10 ppt	Sensitivity needed to assess total radioactive background
R-200002	1.10	Assay Sensitivity for U and Th by Neutron Activation Analysis	1.5 ppt	Sensitivity needed to assess total radioactive background
R-200003	1.10	Assay Sensitivity for U and Th by ICP-MS	10 ppt	Sensitivity needed to assess total radioactive background
R-200004	1.10	Assay Sensitivity for Radon Emanation	0.3 mBq	Sensitivity needed to assess total radioactive background
R-200005	1.10	Assay Sensitivity for ^{210}Pb in the bulk	10 mBq/kg	Sensitivity needed to assess total radioactive background
R-200006	1.10	Assay Sensitivity for ^{210}Pb Plateout	60 nBq/cm^2	Sensitivity needed to assess total radioactive background
R-200007	1.10	Assay Sensitivity for Dust Accumulation	10 ng/cm^2	Sensitivity needed to assess total radioactive background

12.2.11 WBS 1.11 Offline Computing

The primary requirements for WBS 1.11 Offline Computing are shown in Table 12.2.11, and are primarily the amount of disk and CPU to enable adequately detailed studies of the detector and background levels to be performed. Without sufficient computing resources, the project is unable to determine whether it is satisfying the top level science requirements. WBS 1.11 is also critically important in coordinating computing and software tasks with other WBS elements, particularly in simulations and analysis tools.

Table 12.2.11: Level 2 Requirements for WBS 1.11 Offline Computing

Number	WBS	Requirement Name	Requirement Description	Rationale
R-210001	1.11	US Disk Costs FY15-FY18	Procure NERSC GPFS disk for simulation, development, and initial data taking	Handle simulation data, derived data, and user data volumes as defined in Table 11.2.2
R-210002	1.11	US CPU Costs FY15-FY18	Procure NERSC PDSF CPU for simulation, development, and initial data taking	Handle simulation data, derived data, and user data volumes as defined in Table 11.2.2
R-210003	1.11	US Server Costs FY15-FY18	Procure and maintain servers for simulation and development	Handle simulation data, derived data, and user data volumes as defined in Table 11.2.2
R-210004	1.11	UK Data Center	Design, deploy, test, and maintain UK Data Center at Imperial	Handle simulation data, derived data, and user data volumes as described in Sec. 11.2.2

12.3 Sensitivity and Detector Performance

We employ the simulation tools described in Section 12.1 to evaluate the sensitivity of LZ, as defined by the requirements in Section 12.2, to a WIMP signal. Additionally, we evaluate the impact of variations in the parameters that define the LZ apparatus on its sensitivity.

The high-statistics calibrations performed by LUX and their incorporation into NEST have driven a conversion from the simple cut-and-count statistical methods used in the CDR to more advanced likelihood methods. The use of likelihood methods has markedly reduced the sensitivity of LZ to the dominant electron recoil backgrounds. Table 12.3.1 shows the number of counts with S1 signals between 0 and 20 photoelectrons coming from different background sources in a 1,000 d run with no discrimination applied, analogous to Table 9.2.7 (see Sec. 12.1.4 for further discussion of the cuts used to generate these numbers). For the majority of the chapter, we use the PLR method described in Sec. 12.3.1 to exploit the ER/NR discrimination power of liquid xenon to calculate our sensitivity to dark matter.

Table 12.3.1: Backgrounds described by PDFs in the profile likelihood analysis, with the counts expected with S1 signal between 0 and 20 photoelectrons in a 1,000 d run, with no discrimination applied, analogous to Table 9.2.7 (see Sec. 12.1.4 for further discussion of the cuts used to generate these numbers).

Background	Type	Counts
^{8}B solar ν	NR	7
hep ν	NR	0.21
DSN ν	NR	0.05
ATM ν	NR	0.46
pp + ^{7}Be + ^{14}N solar ν	ER	255
^{136}Xe ($2\nu\beta\beta$)	ER	67
^{85}Kr	ER	24.5
^{222}Rn	ER	722
^{220}Rn	ER	122
Detector components + Environmental	ER	11.3
Detector components + Environmental	NR	0.5

Our evaluation of the LZ sensitivity should be considered as a snapshot in time. The field of direct dark matter detection with liquid xenon TPCs continues to achieve increasing sensitivity. Since the completion of the LZ CDR [1], the LUX Collaboration has substantially advanced the understanding of the response of liquid xenon to both background and signal [3, 5], knowledge which has been incorporated in this report. As the LZ construction project progresses, key response and radioactive background properties will be measured and our sensitivity evaluation will adapt. We endeavor to bound this evolution by providing a "baseline" parameter set as well as "goal" and "reduced" sets, summarized in Table 12.3.2. The variation of sensitivity with excursions in many LZ parameters is captured in Section 12.3.3.

12.3.1 Profile Likelihood Ratio Method

The sensitivity projections in this report are based on a profile likelihood ratio (PLR) method [4], which allows near-optimum exploitation of the differences between signal and background in the key parameters that are reconstructed by the LZ apparatus. The parameters with the highest sensitivity to these differences are the position-corrected S1 (primary scintillation light) and S2 (secondary luminescence from ionization) signals. The position of events in radius r and height z also allows distinction between signal and the background events which originate from radioactive impurities in the material in the vicinity of the liquid xenon TPC of LZ; these background events cluster near the edges of the TPC, while the WIMP signal is uniform in the liquid xenon mass. In this report, we apply a simple fiducial volume cut, where 5.6 tonnes of the inner liquid xenon is retained as the sensitive volume. In the future, our sensitivity studies will exploit the distinct spatial distributions of signal and background just as the LUX experiment has done, and the fiducial requirement will become unnecessary.

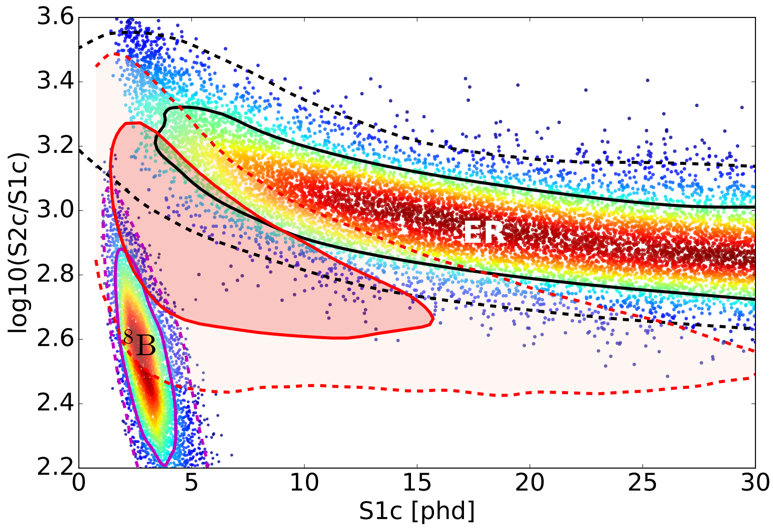

Figure 12.3.1: Simulations of the most prominent ER and NR (from ^{8}B) backgrounds are plotted in the $\log_{10}$(S2c/S1c)-S1c plane. The statistics shown represent 5x the expected ER background and 500x the expected NR background in the nominal LZ exposure. The red tinted area shows the expectation for events from a 40 GeV/c^2-mass WIMP, falling between the two background populations with the region enclosed by the solid(dashed) line representing the $1\,\sigma(2\,\sigma)$ band.

To execute the PLR sensitivity estimate, signal and background probability distribution functions (PDFs) are created in S1 and S2 after application of the fiducial cut in r and z. The signal PDF for each WIMP mass is generated by converting the differential energy spectrum calculated from [20] to S1 and S2 signals in the LZ detector using NEST and the parameterization of detector response described in Section 12.1.3.

The background PDFs are broken into the eleven individual components listed in Table 12.3.1. The simulations for detector components and environmental backgrounds are summed together into a single PDF each for ER and NR events. For each WIMP mass, we scan over the cross section to set a 90 % confidence interval (CI) for the expected number of signal events, evaluated using RooStats [21]. In the PLR technique we use the unbinned likelihood computed in the plane of $\log_{10}$(S2/S1) versus S1. Poisson fluctuations are innate to the technique.

The power of the PLR technique arises from an optimal weighting of the background-free and background-rich regions in the $\log_{10}$(S2/S1)-S1 plane. Figure 12.3.1 shows high-statistics simulations of the most prominent backgrounds (ER events from pp solar neutrinos, ^{222}Rn, and ^{220}Rn, and NR events from ^{8}B neutrinos) in the $\log_{10}$(S2/S1)-S1 plane, representing 5x and 500x the count rates expected in the nominal LZ exposure for ER and NR, respectively. Also shown is the region that would be populated by events from a 40 GeV/c^2 WIMP signal, which falls between the ^{8}B and ER background areas. The PLR technique optimally combines the background-free and background-rich regions. The intense calibrations recently conducted by the LUX collaboration provide confidence in the knowledge of the shapes of the backgrounds and the signal.

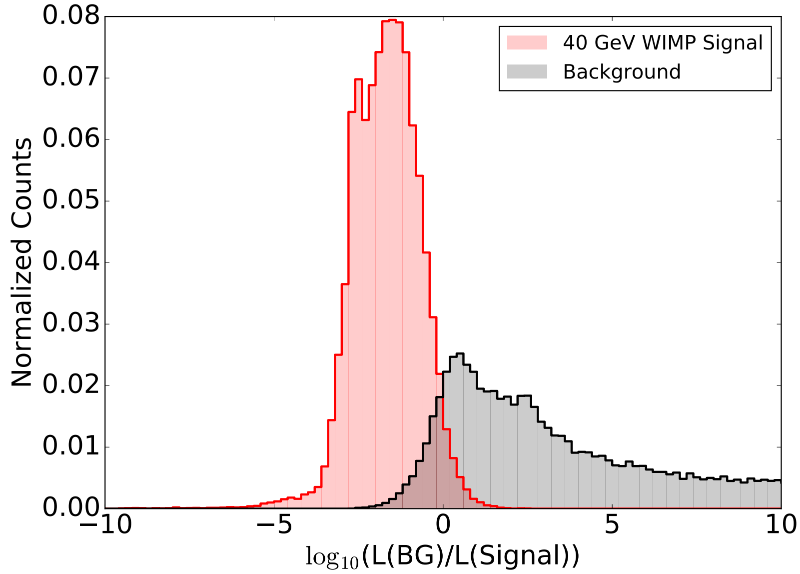

Figure 12.3.2: A one-dimensional projection of the PLR discrimination statistic. Two ensembles of points in the $\log_{10}(S2/S1)$-S1 plane are considered, one distributed like a 40 GeV/c^2 WIMP signal, and the other like the expected background (combining both the ER and ^{8}B bands of Fig. 12.3.1).

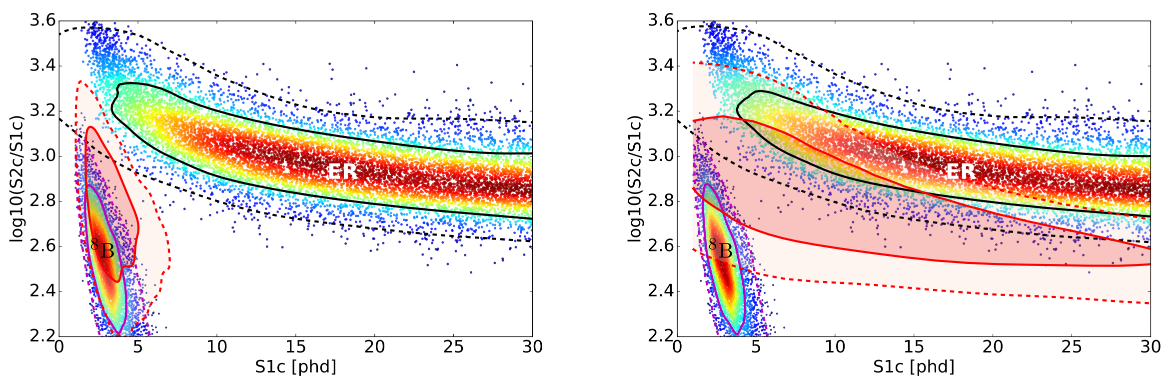

Figure 12.3.3: PLR technique for different masses. The background distributions are the same as in Figure 12.3.1, but the expected signal regions are for a 10 GeV/c^2 WIMP (left) and a 1,000 GeV/c^2 WIMP (right). The signal regions merge, respectively, into the ^{8}B and ER background regions. The expected signal regions are tinted red, with the darker(lighter) color $1\,\sigma(2\,\sigma)$.

The discrimination statistic that quantifies whether each point in the respective ensemble more resembles background or signal is evaluated in one dimension as the difference between logarithms of the likelihoods that a point in the ensemble is background or signal. Low values correspond to poor likelihood to be background, and high values to a good likelihood to be background. Figure 12.3.2 shows the PLR discrimination statistic integrated over the full energy range for a 40 GeV/c^2 WIMP signal and the expected background (combining both the ER and ^{8}B bands of Fig. 12.3.1). Comparison of the two ensembles shows the considerable separation between signal and background available using this method. This plot and similar plots constructed for different WIMP masses are used to describe the discrimination power of the LZ apparatus against background.

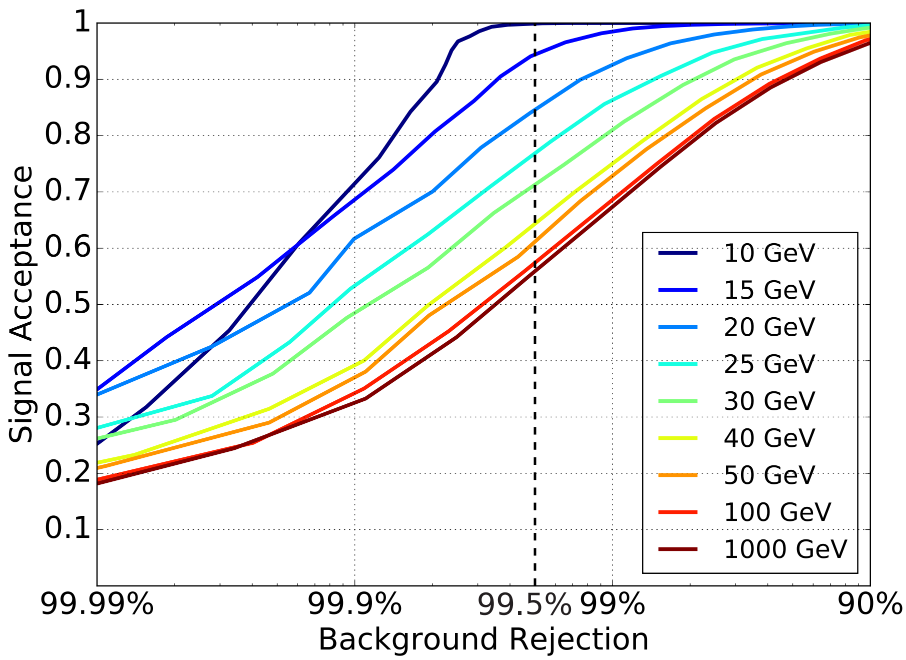

Figure 12.3.4: Acceptance and rejection for WIMP signals in LZ. For a variety of WIMP masses, histograms like that shown in the Fig. 12.3.2 are integrated to derive the curves shown. Backgrounds from both ^{8}B and ER events are included. The requirement of 99.5 % rejection at 50 % acceptance is projected for all WIMP masses.

The expected signal region varies according to the WIMP mass, and Figure 12.3.3 shows the signal regions for WIMP masses of 10 GeV/c^2 and 1,000 GeV/c^2 compared to the same ER and NR simulations of Fig. 12.3.1. The PLR method naturally takes into account the shape of the expected WIMP signal, and the achievable discrimination at all WIMP masses is thus significantly better than that attainable in the 'cut and count' technique utilized in the LZ CDR. Figure 12.3.4 shows the signal acceptance for WIMPs of a variety of masses as a function of the fraction of the background rejected. For all WIMP masses, a background rejection that exceeds 99.5 % for signal acceptance of 50 % is projected.

12.3.2 LZ Sensitivity Projection

To evaluate the projected sensitivity for LZ, we consider a run of 1,000 live days and a 5.6 tonne fiducial mass. We assume the same background models of Table 12.3.1, where background counts were shown for a signal region encompassing 0 to 20 phd, effectively the search region for 100 GeV/c^2 WIMP masses and below. To increase the sensitivity over the entire WIMP mass range, we consider an expanded S1 signal region of 0 to 50 phd, corresponding to 1.5 to 16 keV$_{ee}$ for ER and 6 to 60 keV$_{nr}$ for NR. Although the expanded search region brings with it a higher absolute count of backgrounds than those listed in the table, the use of the PLR method smoothly accounts for the profiles of these backgrounds relative to each WIMP mass as described in the previous section. We include the requirement of a 3-fold coincidence for the PMTs.

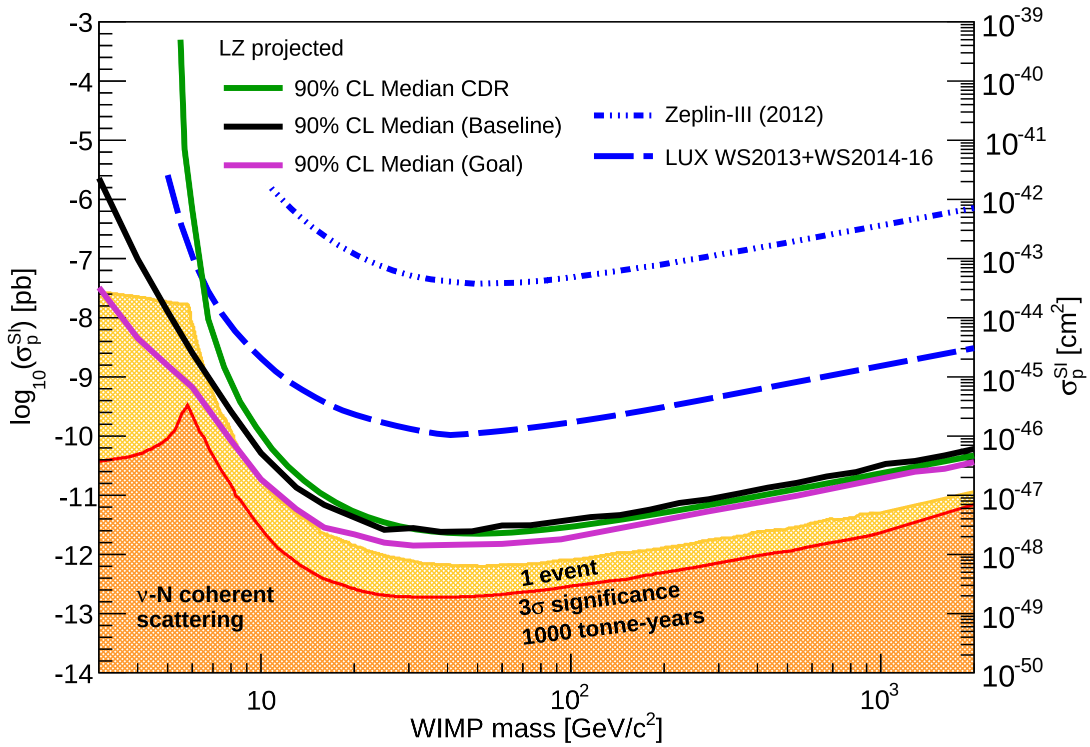

Figure 12.3.5: LZ sensitivity projection. The baseline LZ assumptions in this report give the solid black curve. LUX and ZEPLIN results are shown in broken blue lines. If LZ achieves the design goals listed in Table 12.3.2, the sensitivity would improve, resulting in the pink sensitivity curve. The green line shows the projected sensitivity in the LZ Conceptual Design Report (CDR) [1] (see text for details of the changes from the CDR to this report). Lastly, the shaded regions show where coherent scattering neutrino backgrounds emerge.

The projected sensitivity curve for LZ is shown in Figure 12.3.5. The best sensitivity is 2.3×10^{-48} cm^2 for a 40 GeV/c^2 WIMP mass, which satisfies our top level science requirement.

Figure 12.3.5 also shows the projected sensitivity from the LZ Conceptual Design Report (CDR) [1]. There are three main differences in this projection with respect to the CDR:

1. We have increased the assumed level of ^{222}Rn and ^{220}Rn by a factor of twenty, so radon is now the dominant source of ER events in the detector.

2. The PLR technique as described in the previous section is used to evaluate the dark matter sensitivity, instead of a simple cut and count approach. These two changes effectively offset: there is a higher

overall background level but those backgrounds are more effectively rejected by the analysis technique. Our confidence in the ER background shape, most important for using the PLR technique, rests on the high-statistics LUX tritium ER calibration [2].

3. The LUX neutron calibration results, which allow LZ to more confidently project the response of the detector to very low energy nuclear recoils. Use of the neutron calibration provides the greatly increased sensitivity to very low-mass WIMPs in the new projection.

Figure 12.3.6 shows the discovery potential for LZ under the baseline assumptions, calculated using a cut-and-count technique via the TRolke package [22, 23]. With the baseline parameters, LZ will have 3σ significance for 40 GeV/c^2 WIMP mass at a cross section of 6.0×10^{-48} cm^2. We also show the 5σ significance curve, which falls below the projections from the XENON1T experiment at all WIMP masses. Figure 12.3.7 shows the background and signal events populating the $\log_{10}$(S2/S1)-S1 plane in an example LZ experiment with 1000 days and 5600 kg exposure for the 3σ example combination of WIMP parameters.

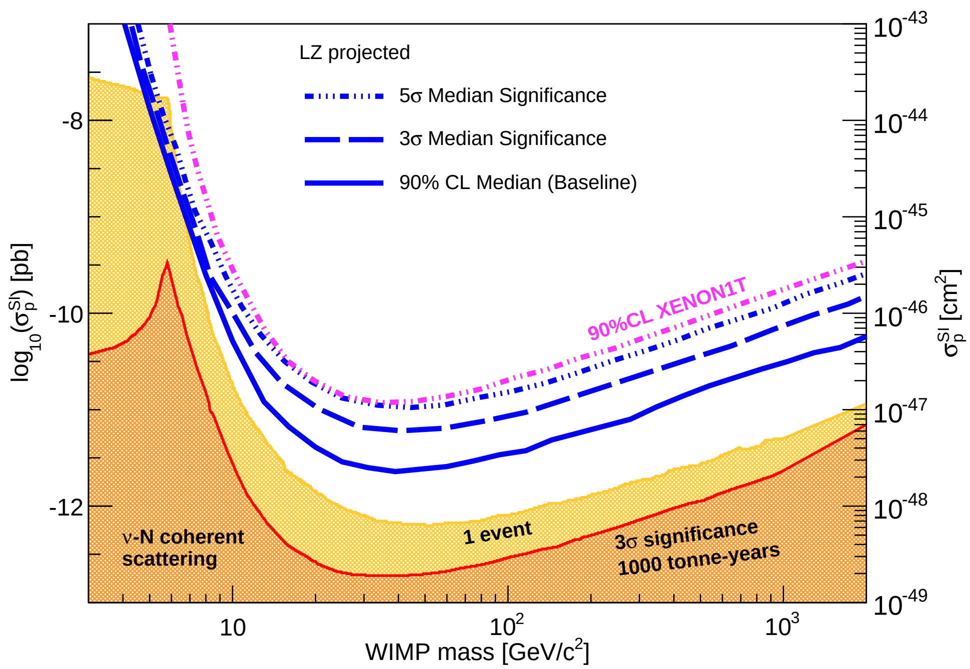

Figure 12.3.6: The discovery potential for LZ under the baseline assumptions, calculated using a cut-and-count technique via the TRolke package [22, 23]. With the baseline parameters, LZ will have 3σ significance for 40 GeV/c^2 WIMP mass at a cross section of 6.0×10^{-48} cm^2. The 5σ significance expectation is just below the expected 90 % CL limit from a two year run of XENON1T at all WIMP masses.

12.3.3 Parameter Scans of LZ Sensitivity

We have explored the dependency of the LZ sensitivity to spin-independent interactions of WIMPs upon critical detector performance assumptions. Our baseline parameters lead to the sensitivity shown by the solid blue curve in Fig. 12.3.5

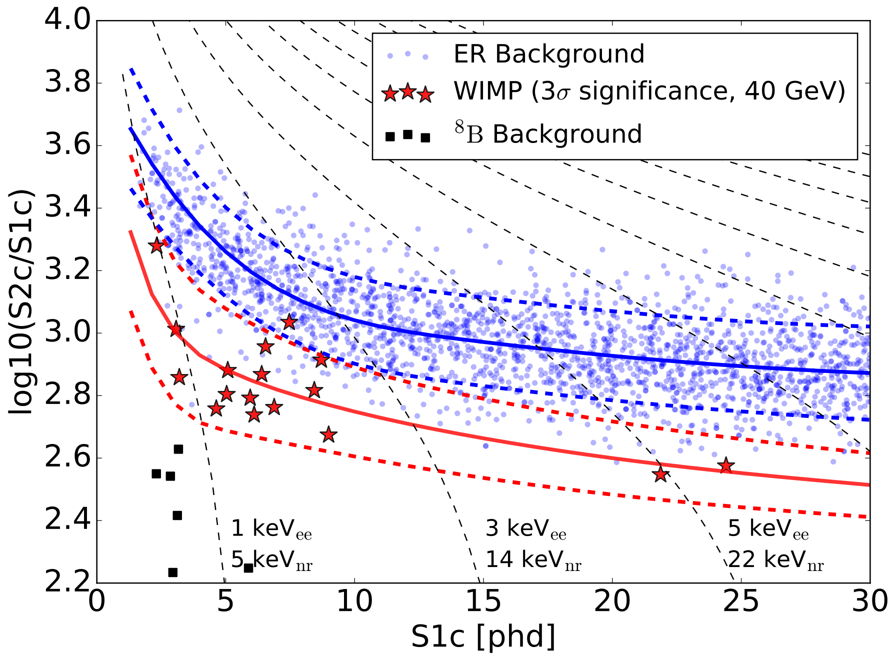

Figure 12.3.7: A sample LZ exposure under the baseline assumptions where the signal represents a 40 GeV/c^2 WIMP mass with a cross section of 6.0×10^{-48} cm^2. LZ will observe several ^{8}B events under these assumptions, along with the nominal ER backgrounds. For these WIMP parameters, LZ will have a 3σ median significance for WIMP discovery. The solid blue and red lines represent the median of the ER and NR bands, the dashed blue and red lines indicate the 10 % to 90 % intervals for each population. The dashed lines running from the top left corner down to the x-axis show lines of constant recoil energy.

One such study defines "goals" as a set of parameters that are likely to be achieved during the fabrication of LZ, but which are somewhat less conservative than the baseline. We define a "reduced" set of parameters as an unlikely worst-case. Both the goal and baseline parameter sets meet all requirements in Section 12.2. These three parameters sets are listed in Table 12.3.2, and their projected performance is shown in Figure 12.3.8. Reaching the LZ goals achieves a sensitivity of 1.1×10^{-48} cm^2 at 40 GeV/c^2. The reduced parameter set degrades the sensitivity to 5.1×10^{-48} cm^2 at 40 GeV/c^2.

Table 12.3.2: Key parameters for reduced, baseline and goal detector performance as explained in the text.

Detector Parameter	Reduced	Baseline	Goal
Light collection (PDE)	0.05	0.075	0.12
Drift field (V/cm)	160	310	650
Electron lifetime (μs)	850	850	2800
PMT phe detection	0.8	0.9	1.0
N-fold trigger coincidence	4	3	2
^{222}Rn (mBq in active region)	13.4	13.4	0.67
Live days	1000	1000	1000

A notable observation that would accompany the achievement of the "goal" set of parameters: over 300 ^{8}B neutrino events would be observed in a 1,000 live days LZ run. While these events would slow the discovery of a WIMP in the 7 GeV/c^2 mass range, they would also demonstrate a physical process not yet observed in nature, the coherent scattering of neutrinos from nuclei.

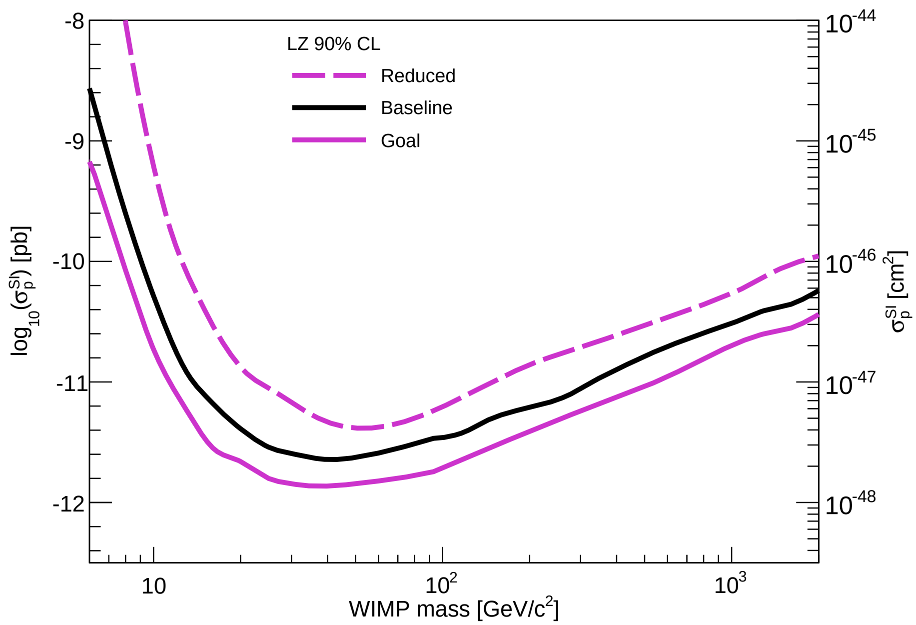

Figure 12.3.8: LZ sensitivity projections for goal, baseline, and reduced parameters. The respective best sensitivities are 1.1×10^{-48} cm^2, 2.3×10^{-48} cm^2 (which both satisfy the primary science requirement), and 5.1×10^{-48} cm^2 at a WIMP mass of 40 GeV/c^2.

In the next several figures, we vary key detector performance parameters to gauge their impact on the median 90 % CL of the upper limit for WIMP cross-section. Figure 12.3.9 shows the impact of ^{222}Rn, the dominant ER background, on LZ sensitivity. Assuming that the goal of 0.67 mBq is achieved, the sensitivity (to a 40 GeV/c^2 WIMP) improves by 20 % over the baseline case. If the Rn background is increased another 10x over the nominal case then the sensitivity would degrade 20 %. The ^{222}Rn rate is representative of a generic flat ER background in LZ. Even a factor of 10 increase in the radon has marginal impact on sensitivity, demonstrating the power of using the PLR to separate ER backgrounds from signal like events. The effect of radon on the discovery potential is more significant, as shown in Fig. 12.3.10, where a 10x increase in the radon rate degrades the discovery potential of the detector by a factor of two.

Figure 12.3.11 shows the impact on sensitivity of scaling the atmospheric (ATM) coherent scattering neutrino background. ATM neutrinos produce nuclear recoils similar to that of a 40 GeV/c^2 WIMP, and their PDF has a high degree of overlap with the WIMP signal. Adjusting the ATM rate serves as a proxy for changing the overall NR count. When the ATM rate is turned up by a factor of 10, it is equivalent to having roughly 5 extra NR counts, degrading the sensitivity (to a 40 GeV/c^2 WIMP) by 25 %.

Figure 12.3.12 shows the effect of changes in the S1 photon detection efficiency alone. Greater light collection leads to better S1 resolution, tightening the distribution of NR and ER events and leading to improved discrimination. Better light collection also improves the low energy threshold of LZ, enhancing sensitivity to low-mass dark matter, although this effect is somewhat countered by also seeing a higher ^{8}B background at low energy. Figure 12.3.13 shows the effect of changes in the purity of the LXe, as represented by the electron lifetime. There is significant margin until the drift time drops below half the baseline value. Figure 12.3.14 gives the dependence on electron extraction efficiency. With only 50 % extraction efficiency, larger fluctuations in the S2 signal lead to a reduction in discrimination power and a corresponding loss of sensitivity. Figure 12.3.15 shows that the sensitivity depends weakly on the drift field. Figure 12.3.16 shows the dependence of the sensitivity on the coincidence trigger requirement, where the baseline design assumes a 3-PMT coincidence trigger. Going to 2-PMT coincidence reduces the threshold and makes a significant impact for low-mass WIMPs and similarly the ^{8}B neutrino signal.

Lastly, Figure 12.3.17 shows how extending the run from 1,000 to 3,000 live days would improve the sensitivity of the experiment. The plot shows the median 90 % confidence level upper limit on the cross section for a 40 GeV/c^2 WIMP. In the baseline case, the sensitivity can be improved from 2.3×10^{-48} cm^2 to 1.3×10^{-48} cm^2. If all the design goals are achieved, the sensitivity can be improved from 1.1×10^{-48} cm^2 to 6×10^{-49} cm^2 with 3,000 live days. Figure 12.3.17 also shows the 1σ bands on the expected sensitivity for both the baseline and goal parameter sets in a given exposure of LZ.

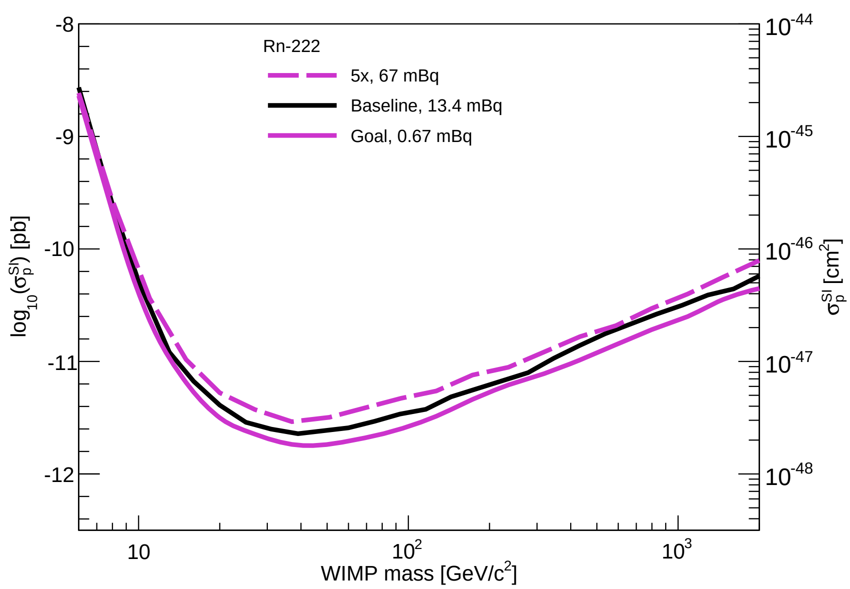

Figure 12.3.9: LZ sensitivity projections for three different assumptions on the concentration of radon in the active volume.

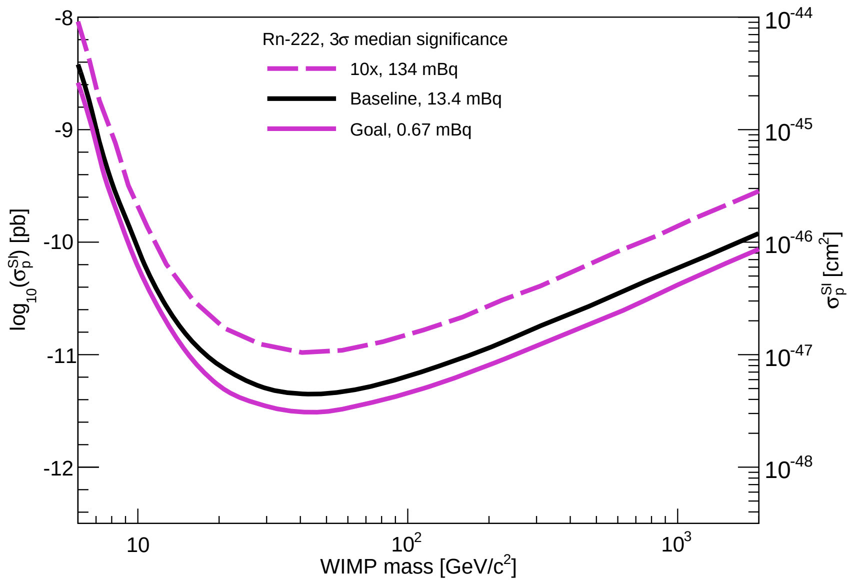

Figure 12.3.10: LZ 3σ median significance projections for three different assumptions on the concentration of radon in the active volume.

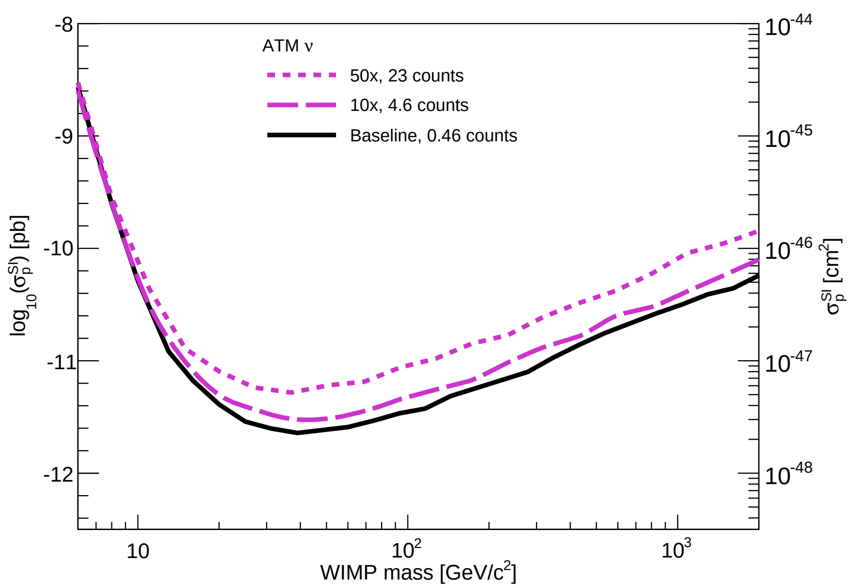

Figure 12.3.11: LZ sensitivity projections vs. scaled atmospheric neutrino flux. Scaling the atmospheric neutrino rate is a proxy for scaling the overall NR backgrounds in LZ.

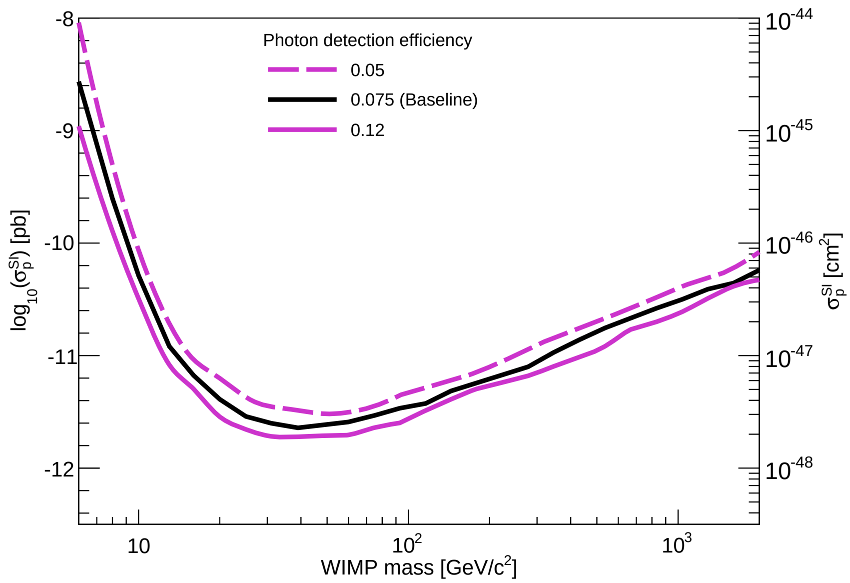

Figure 12.3.12: LZ sensitivity projections vs. S1 photon detection efficiency. We assume a photon detection efficiency of 0.075 for the baseline sensitivity, matching the requirement. The current model of the detector predicts a value of 0.085 (see Sec. 3.5.1).

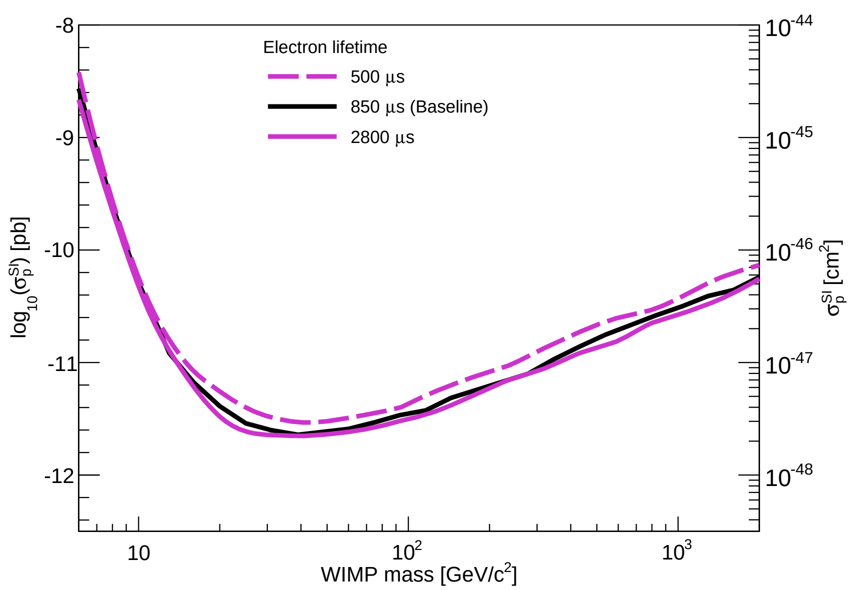

Figure 12.3.13: LZ sensitivity projections vs. electron lifetime (for the nominal electric field value of 310 V/cm). LZ does not lose significant sensitivity until the lifetime drops below half the nominal value of 850 μs.

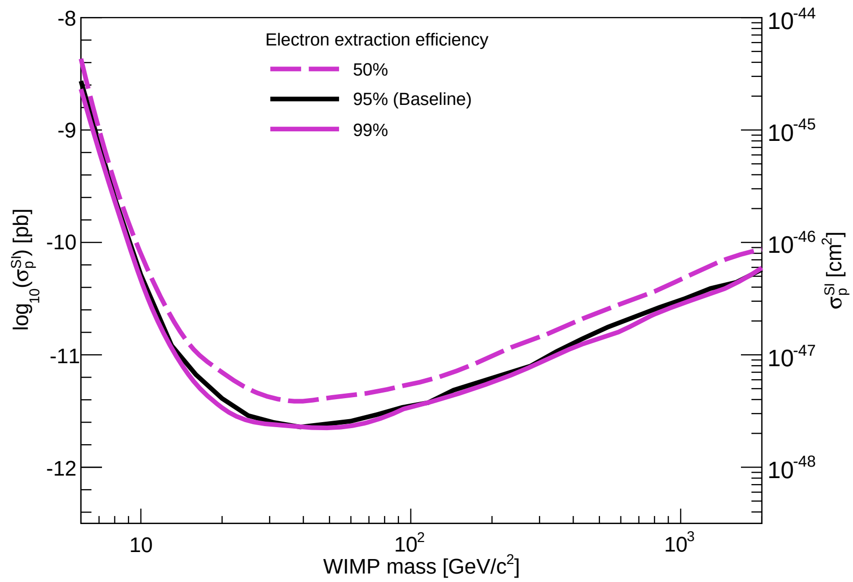

Figure 12.3.14: LZ sensitivity projections vs. electron extraction efficiency. With only 50 % extraction efficiency, larger fluctuations in the S2 signal lead to a reduction in discrimination power and a corresponding loss of sensitivity.

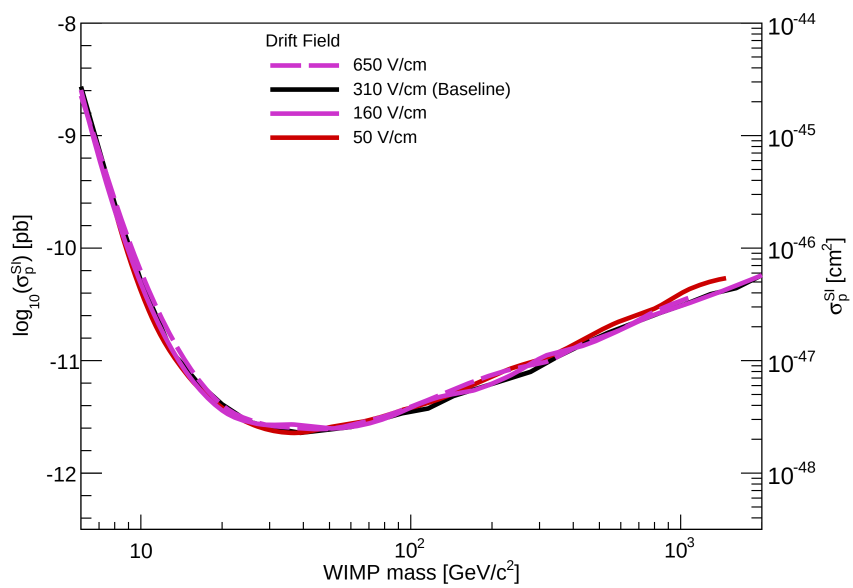

Figure 12.3.15: LZ sensitivity projections vs. electric field. In this regime, the ER/NR discrimination is robust to changes in the drift field, and the effect on sensitivity is minor.

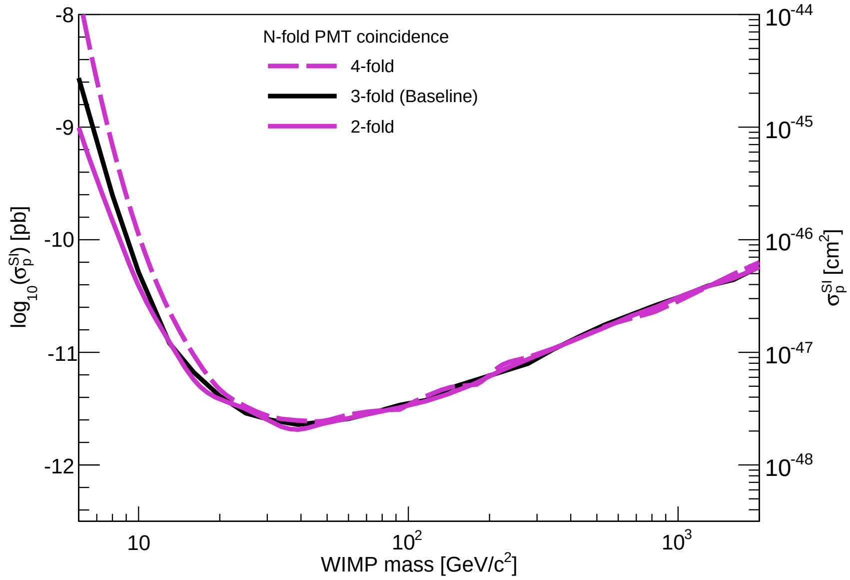

Figure 12.3.16: LZ sensitivity projections vs. trigger coincidence level. The primary effect of the coincidence requirement is on the detection of very low energy events, with direct consequences for sensitivity to low WIMP masses. For comparison, the LUX detector operates with a 2-fold trigger coincidence.

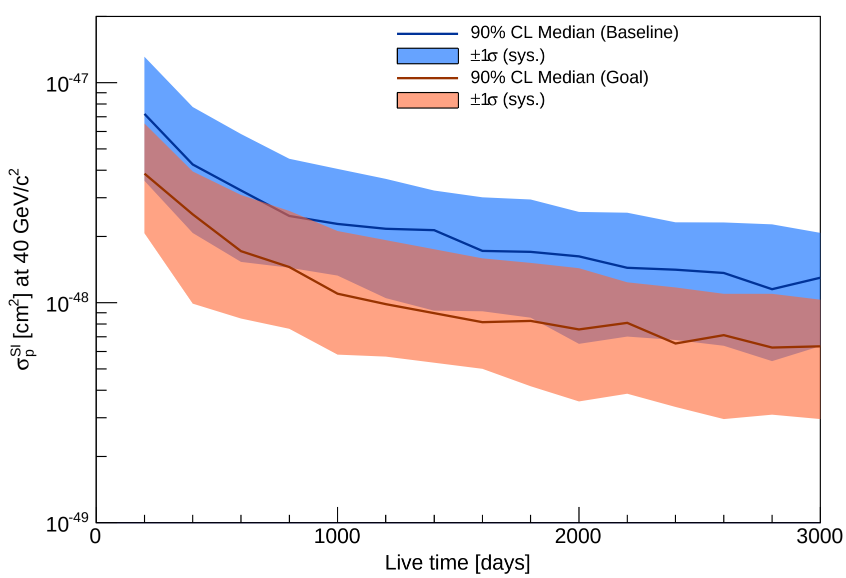

Figure 12.3.17: LZ sensitivity projections vs. exposure for the baseline (blue) and goal (orange). The impact of running the experiment for an additional 2000 days is to improve the sensitivity to 1.2×10^{-48} cm^2 and 6×10^{-49} cm^2 for the baseline and goal scenarios, respectively. Also shown are the 1σ bands showing the range of possible sensitivities for a given exposure.

12.4 Bibliography

[1] D. S. Akerib *et al.* (LZ), (2015), Conceptual Design Report; LBNL-190005, FERMILAB-TM-2621-AE-E-PPD, arXiv:1509.02910 [physics.ins-det].

[2] D. S. Akerib *et al.* (LUX), Phys. Rev. **D93**, 072009 (2016), arXiv:1512.03133 [physics.ins-det].

[3] D. S. Akerib *et al.* (LUX), "Low-energy (0.7-74 keV) nuclear recoil calibration of the LUX dark matter experiment using D-D neutron scattering kinematics," (2016), submitted to Phys. Rev. **C**, arXiv:1608.05381 [physics.ins-det].

[4] G. Cowan, K. Cranmer, E. Gross, and O. Vitells, Eur. Phys. J. **C71**, 1554 (2011), [Erratum: Eur. Phys. J.C73,2501(2013)], arXiv:1007.1727 [physics.data-an].

[5] D. S. Akerib *et al.* (LUX), Phys. Rev. Lett. **116**, 161301 (2016), arXiv:1512.03506 [astro-ph].

[6] D. S. Akerib *et al.* (LUX), Nucl. Instrum. Meth. **A675**, 63 (2012), arXiv:1111.2074 [physics.data-an].

[7] S. Agostinelli *et al.* (GEANT4), Nucl. Instrum. Meth. **A506**, 250 (2003).

[8] M. Szydagis, N. Barry, K. Kazkaz, J. Mock, D. Stolp, M. Sweany, M. Tripathi, S. Uvarov, N. Walsh, and M. Woods (NEST), J. Instrum. **6**, P10002 (2011), arXiv:1106.1613 [physics.ins-det].

[9] M. Szydagis, A. Fyhrie, D. Thorngren, and M. Tripathi (NEST), *Proceedings, LIght Detection In Noble Elements (LIDINE2013)*, J. Instrum. **8**, C10003 (2013), arXiv:1307.6601 [physics.ins-det].

[10] W. B. Wilson *et al.*, *SOURCES4A: A Code for Calculating (alpha,n), Spontaneous Fission, and Delayed Neutron Sources and Spectra*, Tech. Rep. LA-13639-MS (Los Alamos, 1999).

[11] M. J. Carson *et al.*, Astropart. Phys. **21**, 667 (2004), arXiv:hep-ex/0404042 [hep-ex].

[12] R. Lemrani, M. Robinson, V. A. Kudryavtsev, M. De Jesus, G. Gerbier, and N. J. C. Spooner, Nucl. Instrum. Meth. **A560**, 454 (2006), arXiv:hep-ex/0601030 [hep-ex].

[13] V. Tomasello, M. Robinson, and V. A. Kudryavtsev, Astropart. Phys. **34**, 70 (2010).

[14] M. Herman, R. Capote, B. Carlson, P. Oblozinsky, M. Sin, A. Trkov, H. Wienke, and V. Zerkin, Nucl. Data Sheets **108**, 2655 (2007).

[15] V. A. Kudryavtsev, Comput. Phys. Commun. **180**, 339 (2009), (MUSIC), arXiv:0810.4635 [physics.comp-ph].

[16] P. Antonioli, C. Ghetti, E. V. Korolkova, V. A. Kudryavtsev, and G. Sartorelli, Astropart. Phys. **7**, 357 (1997), (MUSIC), arXiv:hep-ph/9705408 [hep-ph].

[17] B. Lenardo, K. Kazkaz, A. Manalaysay, J. Mock, M. Szydagis, and M. Tripathi (NEST), IEEE Trans. Nucl. Sci. **62**, 3387 (2015), arXiv:1412.4417 [astro-ph.IM].

[18] C. E. Dahl, *The physics of background discrimination in liquid xenon, and first results from Xenon10 in the hunt for WIMP dark matter*, Ph.D. thesis, Princeton U. (2009).

[19] C. H. Faham, V. M. Gehman, A. Currie, A. Dobi, P. Sorensen, and R. J. Gaitskell, J. Instrum. **10**, P09010 (2015), arXiv:1506.08748 [physics.ins-det].

[20] C. McCabe, Phys. Rev. **D82**, 023530 (2010), arXiv:1005.0579 [hep-ph].

[21] L. Moneta, K. Belasco, K. S. Cranmer, S. Kreiss, A. Lazzaro, D. Piparo, G. Schott, W. Verkerke, and M. Wolf, *Proceedings, 13th International Workshop on Advanced computing and analysis techniques in physics research (ACAT2010)*, PoS **ACAT2010**, 057 (2010), arXiv:1009.1003 [physics.data-an].

[22] J. Lundberg, J. Conrad, W. Rolke, and A. Lopez, Comput. Phys. Commun. **181**, 683 (2010), arXiv:0907.3450 [physics.data-an].

[23] W. A. Rolke, A. M. Lopez, and J. Conrad, Nucl. Instrum. Meth. **A551**, 493 (2005), arXiv:physics/0403059 [physics].